

## The $^{234}\text{U}$ neutron capture cross section measurement at the n\_TOF facility

C. Lampoudis<sup>1,2,a</sup>, U. Abbondanno<sup>3</sup>, G. Aerts<sup>2</sup>, H. Álvarez<sup>4</sup>, F. Álvarez-Velarde<sup>5</sup>, S. Andriamonje<sup>2</sup>, J. Andrzejewski<sup>6</sup>, P. Assimakopoulos<sup>7</sup>, L. Audouin<sup>8</sup>, G. Badurek<sup>9</sup>, P. Baumann<sup>10</sup>, F. Bečvář<sup>11</sup>, E. Berthoumieux<sup>2</sup>, F. Calviño<sup>12</sup>, M. Calviani<sup>13,14</sup>, D. Cano-Ott<sup>5</sup>, R. Capote<sup>15,16</sup>, C. Carrapiço<sup>2,17</sup>, P. Cennini<sup>18</sup>, V. Chepel<sup>19</sup>, E. Chiaveri<sup>18</sup>, N. Colonna<sup>20</sup>, G. Cortes<sup>21</sup>, A. Couture<sup>22</sup>, J. Cox<sup>22</sup>, M. Dahlfors<sup>18</sup>, S. David<sup>8</sup>, I. Dillmann<sup>23</sup>, C. Domingo-Pardo<sup>23,24</sup>, W. Dridi<sup>2</sup>, I. Duran<sup>4</sup>, C. Eleftheriadis<sup>1</sup>, M. Embid-Segura<sup>5</sup>, L. Ferrant<sup>7,8</sup>, A. Ferrari<sup>18</sup>, R. Ferreira-Marques<sup>19</sup>, K. Fujii<sup>3</sup>, W. Furman<sup>25</sup>, I. Goncalves<sup>19</sup>, E. González-Romero<sup>5</sup>, F. Gramegna<sup>13</sup>, C. Guerrero<sup>5</sup>, F. Gunsing<sup>2</sup>, B. Haas<sup>26</sup>, R. Haight<sup>27</sup>, M. Heil<sup>23</sup>, A. Herrera-Martinez<sup>18</sup>, M. Igashira<sup>28</sup>, E. Jericha<sup>9</sup>, F. Käppeler<sup>23</sup>, Y. Kadi<sup>18</sup>, D. Karadimos<sup>7</sup>, D. Karamanis<sup>7</sup>, M. Kerveno<sup>10</sup>, P. Koehler<sup>29</sup>, E. Kossionides<sup>30</sup>, M. Krtička<sup>11</sup>, H. Leeb<sup>9</sup>, A. Lindote<sup>19</sup>, I. Lopes<sup>19</sup>, M. Lozano<sup>16</sup>, S. Lukic<sup>10</sup>, J. Marganiec<sup>6</sup>, S. Marrone<sup>20</sup>, T. Martínez<sup>5</sup>, C. Massimi<sup>31</sup>, P. Mastinu<sup>13</sup>, A. Mengoni<sup>15,18</sup>, P.M. Milazzo<sup>3</sup>, C. Moreau<sup>3</sup>, M. Mosconi<sup>23</sup>, F. Neves<sup>19</sup>, H. Oberhummer<sup>9</sup>, S. O'Brien<sup>22</sup>, J. Pancin<sup>2</sup>, C. Papachristodoulou<sup>7</sup>, C. Papadopoulos<sup>32</sup>, C. Paradela<sup>4</sup>, N. Patronis<sup>7</sup>, A. Pavlik<sup>33</sup>, P. Pavlopoulos<sup>34</sup>, L. Perrot<sup>2</sup>, M.T. Pigni<sup>9</sup>, R. Plag<sup>23</sup>, A. Plompen<sup>35</sup>, A. Plukis<sup>2</sup>, A. Poch<sup>21</sup>, J. Praena<sup>13</sup>, C. Pretel<sup>21</sup>, J. Quesada<sup>16</sup>, T. Rauscher<sup>36</sup>, R. Reifarh<sup>27</sup>, C. Rubbia<sup>37</sup>, G. Rudolf<sup>10</sup>, P. Rullhusen<sup>35</sup>, J. Salgado<sup>17</sup>, C. Santos<sup>17</sup>, L. Sarchiapone<sup>18</sup>, I. Savvidis<sup>1</sup>, C. Stephan<sup>8</sup>, G. Tagliente<sup>20</sup>, J.L. Tain<sup>24</sup>, L. Tassan-Got<sup>8</sup>, L. Tavora<sup>17</sup>, R. Terlizzi<sup>20</sup>, G. Vannini<sup>31</sup>, P. Vaz<sup>17</sup>, A. Ventura<sup>38</sup>, D. Villamarin<sup>5</sup>, M.C. Vicente<sup>5</sup>, V. Vlachoudis<sup>18</sup>, R. Vlastou<sup>32</sup>, F. Voss<sup>23</sup>, S. Walter<sup>23</sup>, M. Wiescher<sup>22</sup>, and K. Wisshak<sup>23</sup>

The n\_TOF Collaboration (www.cern.ch/ntof)

<sup>1</sup>Aristotle University of Thessaloniki, Greece – <sup>2</sup>CEA/Saclay-DSM/DAPNIA, Gif-sur-Yvette, France – <sup>3</sup>Istituto Nazionale di Fisica Nucleare, Trieste, Italy – <sup>4</sup>Universidad de Santiago de Compostela, Spain – <sup>5</sup>Centro de Investigaciones Energeticas Medioambientales y Tecnológicas, Madrid, Spain – <sup>6</sup>University of Lodz, Lodz, Poland – <sup>7</sup>University of Ioannina, Greece – <sup>8</sup>Centre National de la Recherche Scientifique/IN2P3-IPN, Orsay, France – <sup>9</sup>Atominsttitut der Österreichischen Universitäten, Technische Universität Wien, Austria – <sup>10</sup>Centre National de la Recherche Scientifique/IN2P3-IRES, Strasbourg, France – <sup>11</sup>Charles University, Prague, Czech Republic – <sup>12</sup>Universidad Politecnica de Madrid, Spain – <sup>13</sup>Istituto Nazionale di Fisica Nucleare, Laboratori Nazionali di Legnaro, Italy – <sup>14</sup>Dipartimento di Fisica, Università di Padova, Italy – <sup>15</sup>International Atomic Energy Agency (IAEA), Nuclear Data Section, Vienna, Austria – <sup>16</sup>Universidad de Sevilla, Spain – <sup>17</sup>Instituto Tecnológico e Nuclear (ITN), Lisbon, Portugal – <sup>18</sup>CERN, Geneva, Switzerland – <sup>19</sup>LIP-Coimbra & Departamento de Fisica da Universidade de Coimbra, Portugal – <sup>20</sup>Istituto Nazionale di Fisica Nucleare, Bari, Italy – <sup>21</sup>Universitat Politecnica de Catalunya, Barcelona, Spain – <sup>22</sup>University of Notre Dame, Notre Dame, USA – <sup>23</sup>Forschungszentrum Karlsruhe GmbH (FZK), Institut für Kernphysik, Germany – <sup>24</sup>Instituto de Física Corpuscular, CSIC-Universidad de Valencia, Spain – <sup>25</sup>Joint Institute for Nuclear Research, Frank Laboratory of Neutron Physics, Dubna, Russia – <sup>26</sup>Centre National de la Recherche Scientifique/IN2P3-CENBG, Bordeaux, France – <sup>27</sup>Los Alamos National Laboratory, New Mexico, USA – <sup>28</sup>Tokyo Institute of Technology, Tokyo, Japan – <sup>29</sup>Oak Ridge National Laboratory, Physics Division, Oak Ridge, USA – <sup>30</sup>NCSR, Athens, Greece – <sup>31</sup>Dipartimento di Fisica, Università di Bologna, and Sezione INFN di Bologna, Italy – <sup>32</sup>National Technical University of Athens, Greece – <sup>33</sup>Institut für Isotopenforschung und Kernphysik, Universität Wien, Austria – <sup>34</sup>Pôle Universitaire Léonard de Vinci, Paris La Défense, France – <sup>35</sup>CEC-JRC-IRMM, Geel, Belgium – <sup>36</sup>Department of Physics-University of Basel, Switzerland – <sup>37</sup>Università degli Studi Pavia, Pavia, Italy – <sup>38</sup>ENEA, Bologna, Italy

**Abstract.** The neutron capture cross-section of  $^{234}\text{U}$  has been measured for energies from thermal up to the keV region in the neutron time-of-flight facility n\_TOF, based on a spallation source located at CERN. A  $4\pi$  BaF<sub>2</sub> array composed of 40 crystals, placed at a distance of 184.9 m from the neutron source, was employed as a total absorption calorimeter (TAC) for detection of the prompt  $\gamma$ -ray cascade from capture events in the sample. This text describes the experimental setup, all necessary steps followed during the data analysis procedure. Results are presented in the form of R-matrix resonance parameters from fits with the SAMMY code and compared to the evaluated data of ENDF in the relevant energy region, indicating the good performance of the n\_TOF facility and the TAC.

### 1 Introduction

At an international level several issues accompany the long-term development of nuclear science and its applications: nuclear waste management, new reactor design, increasing safety requirements, public acceptance, etc. This has triggered many new R&D activities, such as Accelerator Driven

Systems or next generation reactor concepts and has also enhanced the ongoing effort to expand and improve the existing nuclear data. Among other measurements, the neutron capture cross section determination for several isotopes related to the thorium based nuclear fuel cycle is of special interest. The  $^{234}\text{U}$  measurements were performed at the n\_TOF facility [1] (CERN) using TAC as the detection device. The neutron beam characteristics [2,3] were determined after applying available detection techniques, in order to have an accurate knowledge of the beam portion that interacts with the sample. The n\_TOF

<sup>a</sup> Presenting author, e-mail: christos.lampoudis@cern.ch

Data Acquisition System [4] was designed on the basis of high performance flash ADCs, making it a hardware dead-time free system capable of recording the full detector event series.

The capture yield is the primary quantity to be determined from the procedure. The accuracy of this process depends on many parameters such as: detection efficiency, canning effect, detector's neutron sensitivity, etc. Thus numerous additional measurements had to be done in order to estimate these parameters and all background components related to the data analysis procedure.

## 2 Experimental setup

The most important features concerning the facility, the detection apparatus and the data acquisition system are listed below, giving special attention to those aspects relevant to our data analysis procedure.

The main characteristics of the proton beam, the lead target, and the neutron beam are underlined below. The proton beam is supplied by the CERN Proton Synchrotron (PS) and is carried up to the spallation target. Features:

- 20 GeV/c momentum corresponding to the maximum attainable energy with a repetition frequency of 1 pulse every 2.4 s,
- single proton bunch intensity of  $7 \times 10^{12}$  protons or  $4 \times 10^{12}$  protons depending on the PS operating status.

Several devices are used to provide additional information about the beam.

The spallation mechanism relies on the highly energetic proton beam hitting on the heavy element target. The neutron production efficiency for one 20 GeV/c proton impinging on a lead target is approximately 300 neutrons. The n\_TOF neutron source is a lead block with a total volume of  $80 \times 80 \times 60 \text{ cm}^3$  [3]. In order to reduce the neutron beam contamination from  $\gamma$ -rays and high energy charged particles produced during the spallation reactions, protons hit on the target at an angle of 10 degrees respect to the TOF tube axis. A 5 cm water layer is surrounding the target as a moderator and a cooling system.

The neutron beam delivers approximately  $10^6$  neutrons per pulse integrated over the whole beam surface, at the sample position. The generated neutrons travel nearly 186 m inside a vacuum tube divided in several sections, with a progressively reduced diameter. The pressure in the vacuum tube is less than 1 mbar. Two collimators are placed at 136 m and 175 m to shape the neutron beam that reaches the Experimental Area (EA). A "sweeping magnet" is used to cut down charged particles contaminating the neutron beam. The energy range is wide, starting from thermal up to several hundreds of MeV.

The  $4\pi$  assembly is formed by 12 pentagonal and 30 hexagonal shaped crystals. However, the total number of crystals at n\_TOF was reduced to 40 in order to have entrance and exit points of the neutron beam tube. Those two removed were of hexagonal shape. Detection efficiency for capture events is nearly 100%. The crystals' energy calibration and resolution were monitored on a regular basis, using proper  $\gamma$ -radioactive sources ( $^{137}\text{Cs}$ ,  $^{60}\text{Co}$ ,  $^{88}\text{Y}$  and  $\text{Pu}+^{13}\text{C}$ ). The measured relative resolution values (FWHM) for the 662 keV and 6.2 MeV lines were 12% and 7% respectively.

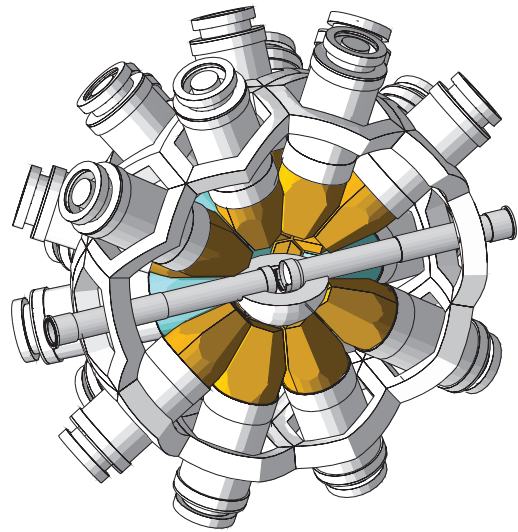


**Fig. 1.** An hemisphere drawing of the TAC sphere as implemented in the Monte Carlo simulation.

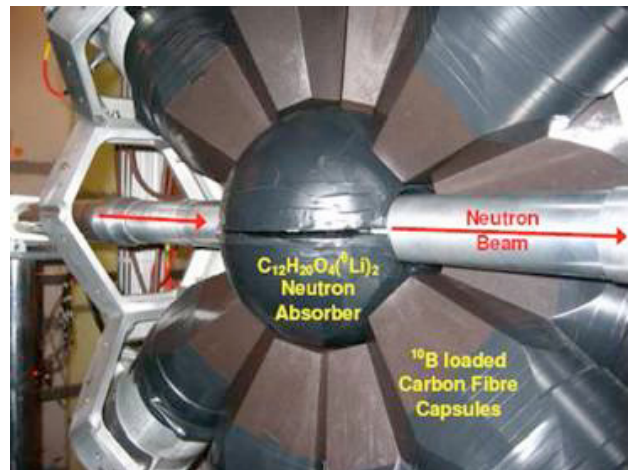


**Fig. 2.** TAC sphere open. Shown, the neutron beam tube entrance unit along with the beam direction and the neutron absorber.

One of the main issues during neutron capture measurements is the detectors' neutron sensitivity. The effect is amplified in the region where  $\sigma_n > \sigma_\gamma$ . In order to reduce the effect a  $\text{C}_{12}\text{H}_{20}\text{O}_4(^6\text{Li})_2$  neutron absorber was employed in the center of the TAC sphere, surrounding the sample. Figure 2 shows the arrangement with the neutron absorber.

## 3 Data analysis

The main aim of the data analysis procedure is the capture yield determination,  $Y(E_n)$ , given by the following formula

$$Y(E_n) = \frac{S(E_n) - B(E_n)}{\Phi(E_n) \cdot \epsilon_{\text{TAC}}(E_n)} \quad (1)$$

where

$S(E_n)$  is the number of events detected in the TAC  
 $B(E_n)$  is the background

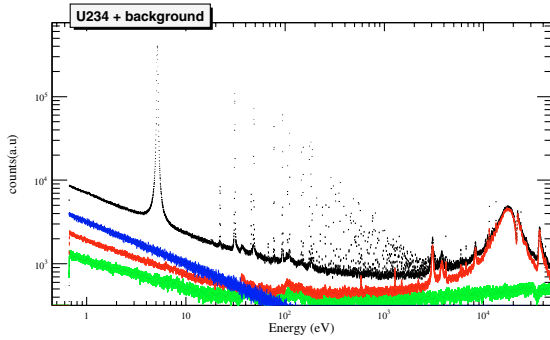


**Fig. 3.** Capture events (arbitrary units) of the  $^{234}\text{U}$  (black) along with the sample's activity (blue), empty Ti canning (red) and empty frame (green).

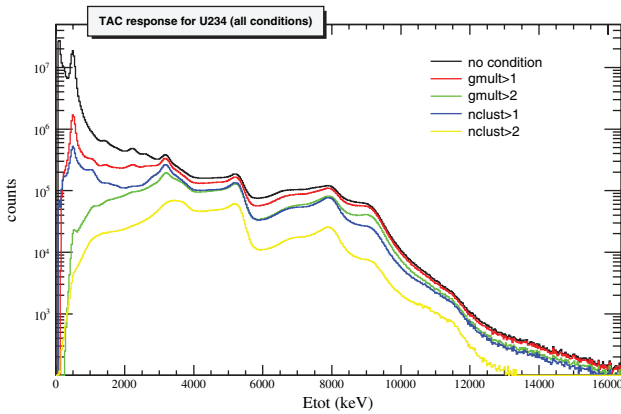


**Fig. 4.** TAC energy response for different conditions.

$\Phi(E_n)$  is the neutron beam flux and  $\epsilon_{\text{TAC}}(E_n)$  is the “global” efficiency of the TAC.

All different sources of background had to be identified and then analyzed regarding their influence on the capture measurements. These are the following:

- as mentioned earlier, background due to neutrons scattered at the samples and captured in the detector materials: mainly in the  $\text{BaF}_2$  and with lower probability, in less abundant surrounding structural materials.
- background due to gamma rays and neutrons emitted in the fission process at the sample. Negligible in our case ( $\sigma_f \ll \sigma_\gamma$ ).
- background due to in-beam gamma rays present in the n\_TOF neutron beam. These are produced by neutrons captured in the hydrogen of the moderator water of the lead spallation target.
- the sample's radioactivity.
- the ambient background.

Several measurements were performed in order to determine each of the previous (fig. 3):

- measuring under the status “beam off”, having just the target inside TAC (sample activity)
- having everything switched off (ambient measurement)
- Carbon sample measurements (TAC neutron sensitivity)
- Lead target measurements (in-beam gammas effect)
- having inside TAC an empty Ti canning.

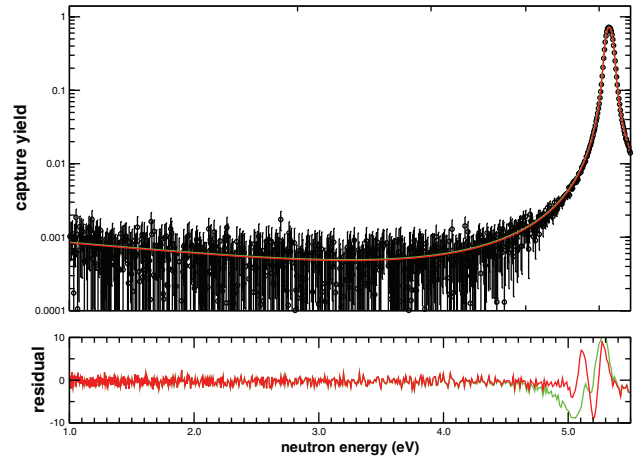


**Fig. 5.** Capture yield (black) along with n\_TOF SAMMY fit (red) and ENDF/B-VI.8 (green) for the first resonance of  $^{234}\text{U}$ .

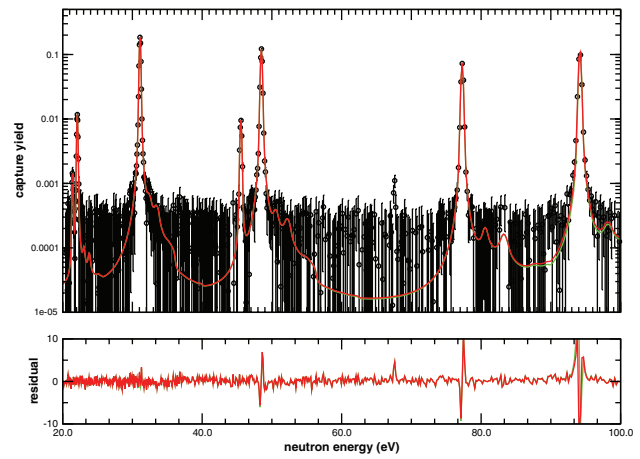


**Fig. 6.** Comparison between experimental data (black), SAMMY fit (red) and ENDF (green) for the neutron energy region up to 100 eV.

Additionally during the analysis, one can apply different selection criteria rules in order to improve signal to background ratio. Defining neighboring crystals as one cluster, we demanded to register events that were detected in two clusters or more ( $N_{\text{cluster}} > 1$ ). This criteria proved to be the best in our case.

The neutron beam flux was estimated by means of Monte Carlo simulations [5] and measured using different available techniques. The neutron flux that was considered in our analysis is the one called n\_TOF standard flux [3].

The last term of equation (1),  $\epsilon_{\text{TAC}}(E_n)$  is called “global” efficiency because it corresponds to the detector's overall efficiency. It is equal to the product of three factors:

**Table 1.** Resonance parameters for the 1st resonance of  $^{234}\text{U}$ .

	$E_n$ (eV)	$\Gamma_\gamma$ (meV)	$\Gamma_n$ (meV)
ENDF/B-VI.8	5.16	40	3.92
JENDL 3.3	5.16	26	3.92
n_TOF	5.156	38.8	3.71

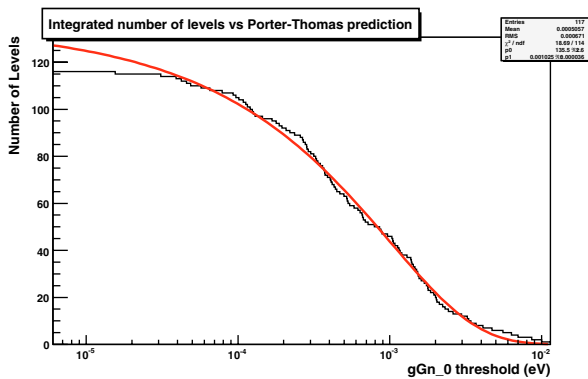


Fig. 7. Number of levels along with the Porter-Thomas distribution fit.

- $\epsilon_\gamma$  is the detector's efficiency, which is close to unity.
- $\epsilon_{\text{beam}}$  the beam portion that interacts with the target. This was found to be equal to 0.1987 from simulations.
- $\epsilon_{\text{condition}}$  a proper coefficient applied, corresponding to the selection criteria used during the analysis process (e.g., energy threshold, multiplicity cuts, etc.). Figure 4 shows the energy response of TAC for various conditions applied, for  $^{234}\text{U}$ .

## 4 Results

For the fitting process of our capture yield, we used the SAMMY software package [6] using ENDF/B-VI.8 resonance parameter set. Prior to the fitting procedure, our capture yield was normalized in order to reproduce the first resonance of  $^{234}\text{U}$ . The comparison between our fit (red) and ENDF/B-VI.8 (green), for the first resonance is shown in figure 5, while figure 6 displays the fit for neutron energy up to 100 eV. In this second plot one can notice a resonance at 67.5 eV, not listed in ENDF/B-VI.8.

The average radiation width was found to be equal to  $40.3 \pm 2.3$  meV, considering resonances up to the energy of 200 eV. The precise number of resonances for the resolved

resonance region was determined after applying the Porter-Thomas distribution on our experimental data (fig. 7). Using that value ( $135.4 \pm 2.6$ ) we calculated the average spacing level,  $\langle D_0 \rangle = 11.04 \pm 0.2$  eV while Mughabghab gives  $10.92 \pm 0.47$  eV [7]. The reduced averaged neutron width obtained from this fit is:  $\langle \Gamma_n^0 \rangle = (1.02 \pm 0.03) \times 10^{-3}$  eV.

## 5 Conclusions

Measurements of the neutron capture in  $^{234}\text{U}$  were performed at the n\_TOF facility (CERN), using the Total Absorption Calorimeter as the detection system. Resonance parameters for the resolved resonance energy region were determined after following the fitting process with SAMMY. Calculations of the average radiation width and mean level spacing validate the good performance of the experimental facility and the adequacy of the data reduction procedure.

We acknowledge the CERN participation in the n\_TOF project. This work has been supported by the European Commission's 5<sup>th</sup> Framework Program under contract FIKW-CT-2000-00107.

## References

1. The n\_TOF Collaboration, Tech. Rep. CERN/INTC 2000-018, CERN, Genève (2000).
2. The n\_TOF Collaboration, Status Report CERN/INTC 2001-021, CERN, Genève (2001).
3. The n\_TOF Collaboration, Performance Report CERN/INTC 2002-037, CERN, Genève (2002).
4. U. Abbondanno, the n\_TOF Collaboration, Nucl. Instrum. Meth. A **538**, 692 (2005).
5. The n\_TOF Collaboration, Tech. Rep. CERN/INTC 2000-016, CERN, Genève (2000).
6. N. Larson, Tech. Rep. ORNL/TM-9179/R7/Draft, Oak Ridge National Laboratory (2006).
7. S. Mughabghab, *Atlas of Neutron Resonances*, Vol. 1, 5th edn. (Elsevier, 2006).